AN EXPERIMENTAL STUDY OF THE EFFECT OF STAINLESS STEEL CLADDING ON THE STRUCTURAL INTEGRITY OF FLAWED STEEL PLATES IN BENDING*

S. K. Iskander, R. K. Nanstad, G. C. Robinson, and C. B. Oland

Metals and Ceramics Division
Oak Ridge National Laboratory
P.O. Box 2008
Oak Ridge, Tennessee 37831

CONF-890721--11

DE89 008735

ABSTRACT

A small crack near the inner surface of clad nuclear reactor pressure vessels is an important consideration in the safety assessment of the structural integrity of the vessel. Experimental results from tests on large clad and unclad plate specimens with surface flaws have shown that (1) a tough surface layer composed of cladding and/or heat-affected zone has arrested running flaws in clad plates under conditions where unclad plates have ruptured, and (2) the residual load-bearing capacity of clad plates with large subclad flaws significantly exceeded that of an unclad plate. The fracture surfaces of unclad plates suggest that the flaw evolves through alternately tunneling then breaking to the surface. In the case of clad plates, it is hypothesized that the tough, strong surface layer inhibits the tunneled flaw from propagating to the surface.

---

*Research sponsored by the Office of Nuclear Regulatory Research, Division of Engineering, U.S. Nuclear Regulatory Commission under Interagency Agreement DOE 1886-8011-9B with the U.S. Department of Energy under contract DE-AC05-840R21400 with Martin Marietta Energy Systems, Inc.

NOMENCLATURE

b/a	Ratio of major to minor axes length of elliptical flaw, see Fig. 1
CP-*n*	Clad plate number *n*
CVN	Charpy V-notch
EB	Electron beam
HAZ	Heat-affected zone
K_I	Mode I plane strain stress intensity factor
ORNL	Oak Ridge National Laboratory
PTS	Pressurized thermal shock
RPV	Reactor pressure vessel

INTRODUCTION

A small crack near the inner surface of clad nuclear reactor pressure vessels (RPVs) is an important consideration in the safety assessment of the structural integrity of the vessel. The aim of the experiments was to determine the behavior of small flaws in the vicinity of a tough surface layer of stainless steel weld overlay cladding. There are considerable experimental results which have shown that, *in the absence of cladding*, a small surface flaw in an embrittled material subjected to severe thermal shock will become a long flaw [1]. However, questions remain about the role tough surface cladding will play in preventing the propagation of small flaws along the surface. Furthermore, the flaw could tunnel beneath the cladding, in which case the residual strength of the structure needs to be estimated. The question is of more than academic interest, since a small crack near the inner surface of clad nuclear RPVs is an important consideration in the safety assessment of the structural integrity of the vessel. The behavior of such flaws is relevant to the pressurized thermal shock (PTS) scenario and to the plant life extension issue.

There is a dearth of information on the behavior of small flaws in the presence of cladding. This has led at least one RPV integrity study [1] to assume infinitely long flaws (although small flaws are certainly more credible). To date, it is difficult to predict the behavior of finite length flaws for various reasons. An important one is that no criteria exist to predict the evolution of the flaw geometry; thus, only general qualitative estimates can be made in terms such as "there is a tendency for the crack to propagate along the surface." Another important reason is the analytical complexity introduced by the three-dimensional nature of finite length flaws. Figure 1 shows the variation of the stress intensity factor K_I for an elliptical flaw as a function of the aspect ratio of the major to minor axes (b/a) for the conditions pertaining to the thermal shock experiment experiment TSE-7 [2].

These curves show that for the initial 19-mm radius, semicircular surface flaw used (b/a = 1), the stress intensity factor at the bottom of the flaw is less than that at the surface until b/a exceeds 3. Thus, such a flaw has a tendency to propagate on the surface before it can increase in depth. This has indeed been verified experimentally: Fig. 2 shows the extensive propagation and bifurcation on the surface of the TSE-7 cylinder originating from the semicircular surface flaw [2]. The flaw also increased in depth to the values shown at selected locations in Fig. 2. It is now an article of faith in the Oak Ridge National Laboratory's (ORNL) Heavy Section Steel Technology program that, in the absence of cladding, a short flaw will grow to become a long one.

The central question to be investigated is whether a relatively thin layer of tough cladding can redistribute the stresses in its immediate vicinity sufficiently to retard crack propagation that would have otherwise occurred. In particular, could cladding arrest an initially short flaw that is propagating along the surface and keep it from becoming a long flaw? Should that occur, then the flaw cannot grow in depth to challenge the integrity of the plate without a significant increase of load beyond that needed to rupture unclad plates. A clad plate research program was conducted as part of ORNL's Heavy Section Steel Technology program in order to investigate the behavior of small flaws in the presence of cladding. The objectives of this research were achieved by comparing the load-bearing capacity of clad and unclad flawed plates.

EXPERIMENT DESCRIPTION AND RESULTS

A plate specimen made of a typical RPV steel conforming to the chemistry of ASTM A 533 grade B has been developed to investigate the effects of cladding on the behavior of flaws (see Fig. 3). The plate from which the specimens were manufactured was given a special heat treatment to raise its transition temperature. Instead of the normal quenching followed by tempering, the plate was first normalized at 1032°C for 2 h and air cooled. The plate was then clad and given the milder-than-usual post-weld heat treatment of 10 h at 593°C, which tempered it only slightly. It was commercially clad using the three-wire series-arc technique with stainless steel types 308, 309, and 312 weld wires. This three-wire series-arc technique was used in some of the older vessels. The ferrite number ranged from 4 to 6 as measured using a Ferrite Scope on broken Charpy V-notch (CVN) specimens.

An electron-beam (EB) weld is introduced into the base metal to provide a crack initiation site and, at

the time a sharp flaw is required, the EB-weld site is hydrogen charged [3,4]. The plate is loaded in four-point bending as shown schematically by the row of arrows in Fig. 3 to approximate the stress gradients due to PTS.

The experiments were performed in two slightly different modes of loading that depended on whether the plate was initially *unflawed* or *flawed*. Tests were performed on six initially *unflawed* plates which were hydrogen charged after the target load was reached and maintained constant. This mode of testing will be termed an "arrest" test, since its purpose was to determine the arrest capacity of clad plates with various amounts of stored energy. The flaw, once it initiated from the EB-weld region, either arrested or ruptured the plate. Plates which did not rupture were heat-tinted at 250 to 325°C to define the arrested flaw shape and were then reloaded until either another pop-in or plate rupture occurred. Tests were also performed on two plates with flaws initiated by hydrogen charging before the plate was loaded. The purpose of tests performed on plates with pre-existing cracks ("initiation" tests) is to determine the residual load-carrying capacity of flawed plates.

Arrest Type Experiments

The target surface strains and corresponding loads for the six plates tested are given in Table 1. For applicable cases the "arrest" load, the load the specimen can support after pop-in, is also given. The surface strain (in the uniform bending moment span of the plate) was the independent parameter used in the selection of the target load. All arrest experiments were performed at either -25 or 25°C, and Fig. 4 shows the point on a typical load vs surface strain curve at which the six plates have been tested. Plate designations shown on the left side of the curve were tested at -25°C, and those on the right side were tested at 25°C. The loads (and strains) were maintained constant under machine stroke control during the period of hydrogen charging and are a measure of the crack driving force (or the potential energy stored in the plate) acting during the instant the flaw initiated in the EB weld. After the initial "arrest" experiment, the plates were heat-tinted to define the arrested flaw shape and reloaded until the pre-existing flaw either popped-in or the plate ruptured. These results are also given in Table 1, together with the test temperatures.

For the first clad plate tested, CP-15, the surface strain was chosen to be approximately the yield strain of the base metal. The plate did not rupture. The target surface strain was increased for plates CP-17 and CP-19. In all three cases, the flaw initiated and arrested after propagating beneath the cladding a

distance that increased with increasing target strain. An unclad plate, CP-21, ruptured when loaded to approximately the base metal yield strain at the surface. The pop-in, arrest loads, and corresponding crack lengths for the four plates tested at room temperature are shown schematically in Fig. 5. It may be noted that as the potential energy stored in the plate increased, the length of the arrested flaw also increased as indicated schematically by the shaded flaw shape in Fig. 5. A photograph of the fracture surface of one of the plates, CP-17, is shown in Fig. 6. The darker area at the center of the broken halves of the plate is the arrested flaw after it has been heat tinted. From this photograph, it may be noted that the surface layer composed of heat-affected zone (HAZ) and cladding arrested the flaw and prevented its propagation along the surface, causing it to tunnel below the surface. This has occurred in almost every clad plate tested. Full details can be found in Ref. 5.

The remaining two clad plates, CP-18 and CP-20, were tested at -25°C in order to obtain data at 50 K below the test temperature for plates CP-15, CP-17, CP-19, and CP-21 and the results are presented later.

Initiation Type Tests on Plates CP-16 and CP-22

The loads at various events for clad plate CP-16 and unclad plate CP-22 are shown in Table 2. Recalling that these two plates were tested with pre-existing flaws, it is interesting to note that the pop-in load (703 kN) for plate CP-16 is within 5% of the target load (676 kN), chosen on the basis of yielding at the surface of base metal, for the "arrest" test for unflawed plate CP-15. The arrested crack shapes are also very similar. Almost the same loads have lead to rupture in both the unclad plates tested, 676 and 689 kN for CP-21 and CP-22, respectively. The fracture surfaces of plates CP-16 and CP-22 from the initiation tests and those of plates CP-15 and CP-21 from the arrest tests are very similar and have been presented elsewhere [6].

DISCUSSION

Initiation and Arrest Type Tests

The tough surface layer of cladding and HAZ seemed to have contributed significantly to the load-bearing capacity of the plates by arresting flaws at loads and temperatures that have ruptured unclad plates, as seen from Tables 1 and 2. For example, in the test on clad plate CP-15, the flaw initiated at a load of 676 kN and arrested at 654 kN, while a load of 676 kN lead to the complete rupture of unclad plate CP-21. In fact, clad plate CP-19 arrested a flaw subjected to a driving force (as measured by the target load of 987 kN) almost 50% higher than that which broke an unclad plate (676 kN).

The load that would rupture a clad plate at room temperature was not determined because it may have exceeded test machine capacity. The bounding of the arrest load at -25°C has been accomplished and is given below. Using the latter results, it can be assumed that it is slightly more than the highest arrest load measured, 987 kN for clad plate CP-19.

As may be seen in Table 1, the arrest load (649 kN) for clad plate CP-18 (676 kN) is just 4% lower than the load that ruptured unclad plate CP-21, even though the temperature was some 50 K lower. Moreover, the rupture load (868 kN) of clad plate CP-20 at -25°C is only 5% higher than the corresponding pop-in load (823 kN) that lead to arrest for clad plate CP-18. Thus, it can be assumed that the load-arresting capacity of clad plates at -25°C is approximately 800 kN.

As may be noted from Tables 1 and 2, the residual load-bearing capacity of plates, as measured by the critical loads in initiation experiments with fairly large flaws, was generally greater than that required to break the unclad plate, even though the test temperatures were lower by 50°C.

Both cladding and HAZ played a prominent role in enhancing the load-carrying capacity of the clad plates. This can be explained by examining the CVN impact energy of the three metallurgical zones of the clad plate specimens: cladding, HAZ, and base metal (see Fig. 7). The HAZ is the toughest of the three metallurgical zones at 25°C, while the cladding appears to be toughest at -25°C. CVN impact energy tests were performed on the cladding, HAZ, and base metal with specimens oriented in a direction corresponding to the EB-induced flaw propagating along the surface of the clad-plate specimens. Results of CVN impact testing on specimens oriented in a direction corresponding to the EB-induced flaw propagating in the thickness orientation were similar [7]. Figure 7 shows that the cladding has a substantially lower ductile-to-brittle transition temperature than base metal as measured by the Charpy impact energy.

It is not clear at this time whether cladding alone, without benefit of the tough strong HAZ, would have also elevated the load-bearing capacity beyond that of the unclad plate. Although data which is directly applicable is meager, in RPVs subjected to radiation-embrittlement, the HAZ will most likely undergo toughness degradation similar to that of the base metal, and would, therefore, not play such a prominent role in arresting propagating flaws [8].

Tunneling Behavior of Finite Length Surface Flaws

Examination of the fracture surfaces suggests a propensity for propagating flaws to tunnel, even without the tough surface layer composed of cladding/HAZ. The

differing "textures" of the fracture surfaces of both unclad plates suggest that the crack front first propagates below the surface, leaving a sharp pointed wedge-shaped unbroken ligament between the flaw and the surface. This ligament then cleaves when the stresses become sufficiently high and re-establishes a through-crack, approximately elliptically shaped. The crack front propagates again below the surface, and the process repeats. This sequence of events appears to have occurred in both unclad plates CP-21 and CP-22. This potential for tunneling is due to the critical stress intensity factor occurring somewhat below the surface because of the lack of constraint on the surface. It is hypothesized that a strong and tough surface layer, such as is the case in these plates, inhibits the flaw from propagating along the surface and, thereby, enhances the load-carrying capacity of the plates.

CONCLUSIONS

Experimental results from tests on large clad and unclad plate specimens with surface flaws have shown that (1) a tough surface layer composed of cladding and HAZ has arrested running flaws in clad plates under conditions where unclad plates have ruptured, and (2) the residual load-bearing capacity of clad plates with large subclad flaws significantly exceeded that of an unclad plate. The fracture surfaces of unclad plates suggest that the flaw evolves through alternately tunneling then erupting to the surface. In clad plates, it is hypothesized that the tough, strong surface layer inhibits the tunneled flaw from erupting to the surface.

ACKNOWLEDGMENTS

The authors wish to acknowledge the contributions made by K. V. Cook and D. J. Alexander in reviewing this paper, as well as B. Q. Atkinson for preparing the manuscript for publication.

REFERENCES

1. Iskander, S. K., "A Method of LEFM Analysis of RPV During SBLOCA," *Int. J. Pressure Vessels Piping* 25, date, 279-98.

2. Cheverton, R. D. et al., *Pressure Vessel Fracture Studies Pertaining to the PWR Thermal-Shock Issue: Experiment TSE-7*, NUREG/CR-4304 (ORNL-6177), Oak Ridge National Laboratory, date.

3. Canonico, D. A. and Hudson, J. D., "Technique for Generating Sharp Cracks in Low-Alloy High Strength

Steels," *Heavy-Section Steel Technology Program Semiann. Prog. Rep. for Period Ending February 28, 1971*, ORNL-4681, Oak Ridge National Laboratory, December 1971, 60-4.

4. Holz, P. P., *Flaw Preparations for HSST Program Vessel Fracture Mechanics Testing: Mechanical-Cyclic Pumping and Electron-Beam Weld-Hydrogen-Charge Cracking Schemes*, NUREG/CR-1274 (ORNL/NUREG/TM-369), Oak Ridge National Laboratory, **date**.

5. Iskander, S. K. et al., "Crack Arrest Behavior in Clad Plates," *Heavy-Section Steel Technology Program Semiann. Prog. Rep. April-September 1987*, NUREG/CR-4219, Vol. 4, No. 2 (ORNL/TM-9593/V4&N2), Oak Ridge National Laboratory, **date**, 222-42.

6. Iskander, S. K. et al., "Crack Arrest Behavior in Clad Plates," *Heavy-Section Steel Technology Program Semiann. Prog. Rep. October 1987-March 1988*, NUREG/CR-4219, Vol. 5, No. 1 (ORNL/TM-9593/V5&N1), Oak Ridge National Laboratory, **date**, 212-26.

7. Iskander, S. K. et al., "Crack Arrest Behavior in Clad Plates," *Heavy-Section Steel Technology Program Semiann. Prog. Rep. October 1986-March 1987*, NUREG/CR-4219, Vol. 4, No. 1 (ORNL/TM-9593/V4&N1), Oak Ridge National Laboratory, **date**, 169-73.

8. Canonico, D. A., "Significance of Reheat Cracks to the Integrity of Pressure Vessels for Light-Water Reactors," *Weld. J. Res. Suppl.* 57(5), May 1979, 127-s-42-s.

Fig. 1. Variation of the stress intensity factor K_I for an elliptic flaw as a function of the aspect ratio of the major to minor axes (b/a). *Source:* Cheverton, R. D. et al., *Pressure Vessel Fracture Studies Pertaining to the PWR Thermal-Shock Issue: Experiment TSE-7*, NUREG/CR-4304 (ORNL-6177), Oak Ridge National Laboratory, **date** 1985.

Fig. 2. Developed view of inner surface of the TSE-7 cylinder in which the 19-mm-radius, semicircular flaw propagated on the surface to become a long flaw during the test. *Source:* Cheverton, R. D. et al., *Pressure Vessel Fracture Studies Pertaining to the PWR Thermal-Shock Issue: Experiment TSE-7*, NUREG/CR-4304 (ORNL-6177), Oak Ridge National Laboratory, **date** 1985.

Fig. 3. Clad plate specimen with electron-beam weld tested in four-point bending.

Fig. 4. Point on load vs surface strain curve at which the six plates were tested in the "arrest" mode. Note that all plates whose designation appear above the curve were tested at -25°C, while those below the curve were tested at 25°C.

Fig. 5. Initiation loads, arrest loads, and corresponding crack lengths for the four plates tested at room temperature.

Fig. 6. Fracture surfaces of clad plate CP-17. The dark areas result from the heat-tinting after testing and show the arrested flaw shape. The scale may be estimated from the 50-mm plate thickness.

Fig. 7. Charpy impact energy of base metal, HAZ, and cladding used in the clad plates. Specimen orientation corresponds to EB-induced flaw propagating along the surface.

Table 1. Target surface strains and corresponding loads for the six plates tested.

Plate	Condition	Type of test[a]	Test temperature[b] (°C)	Load (kN)		Target surface strain (%)
				Pop-in	Arrest[c]	
CP-15	Clad	A	RT	676	654	0.31
		I	-25	759	709	
		I	-100	600	R	
CP-17	Clad	A	RT	890	823	0.45
	Several pop-ins occurred before rupture	I	-25	756/725	R	
CP-19	Clad	A	RT	987	689	0.65
		I	-50	703	R	
CP-21	Unclad	A	RT	676	R	0.27
CP-18	Clad	A	-25	823	649	0.39
		I	-25	698	R	
CP-20	Clad	A	-25	868	R	0.41

[a] A = arrest, I = initiation.

[b] RT = room temperature, approximately 25°C.

[c] R = plate ruptured in two pieces.

Table 2. Summary of initiation and arrest loads for plates CP-16 and CP-22.

Plate	Condition	Test temperature (°C)	Load (kN)	
			Initiation	Arrest
CP-16	Clad	21	703	694
		21	890	738
		-25	698	Rupture
CP-22	Unclad	21	698	Rupture

FIG. 1

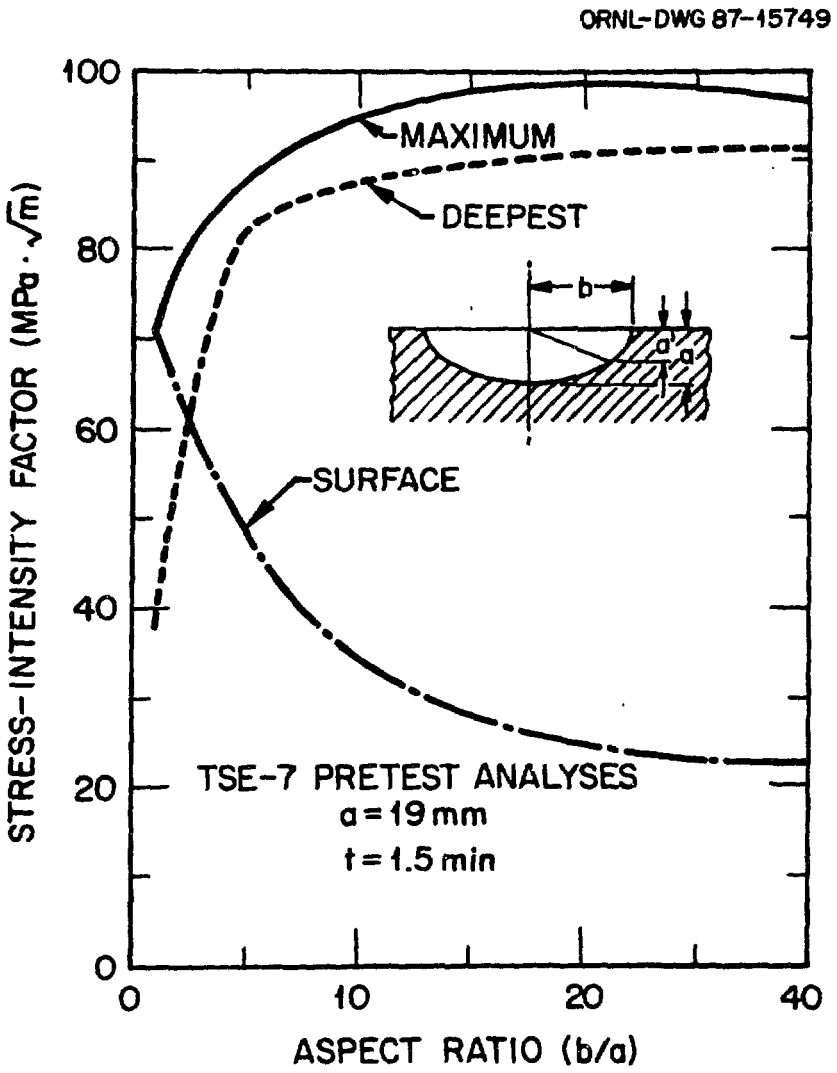
ORNL-DWG 87-15749
STRESS-INTENSITY FACTOR (MPa·√m)
ASPECT RATIO (b/a)
MAXIMUM
DEEPEST
SURFACE
b
a
a
TSE-7 PRETEST ANALYSES
a = 19 mm
t = 1.5 min
0
20
40
60
80
100
0
10
20
40

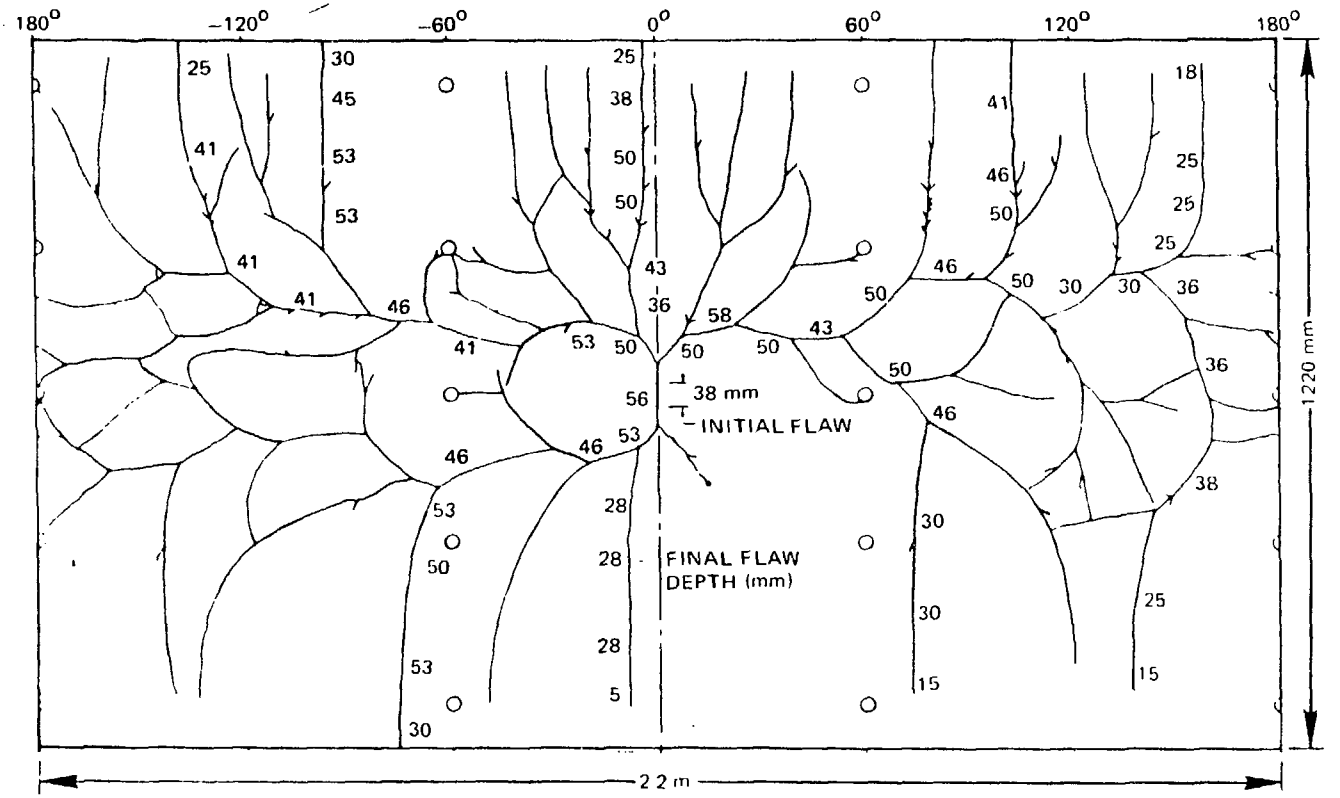

ALL DIMENSIONS IN MILLIMETERS

TSE-7

Fig. 3

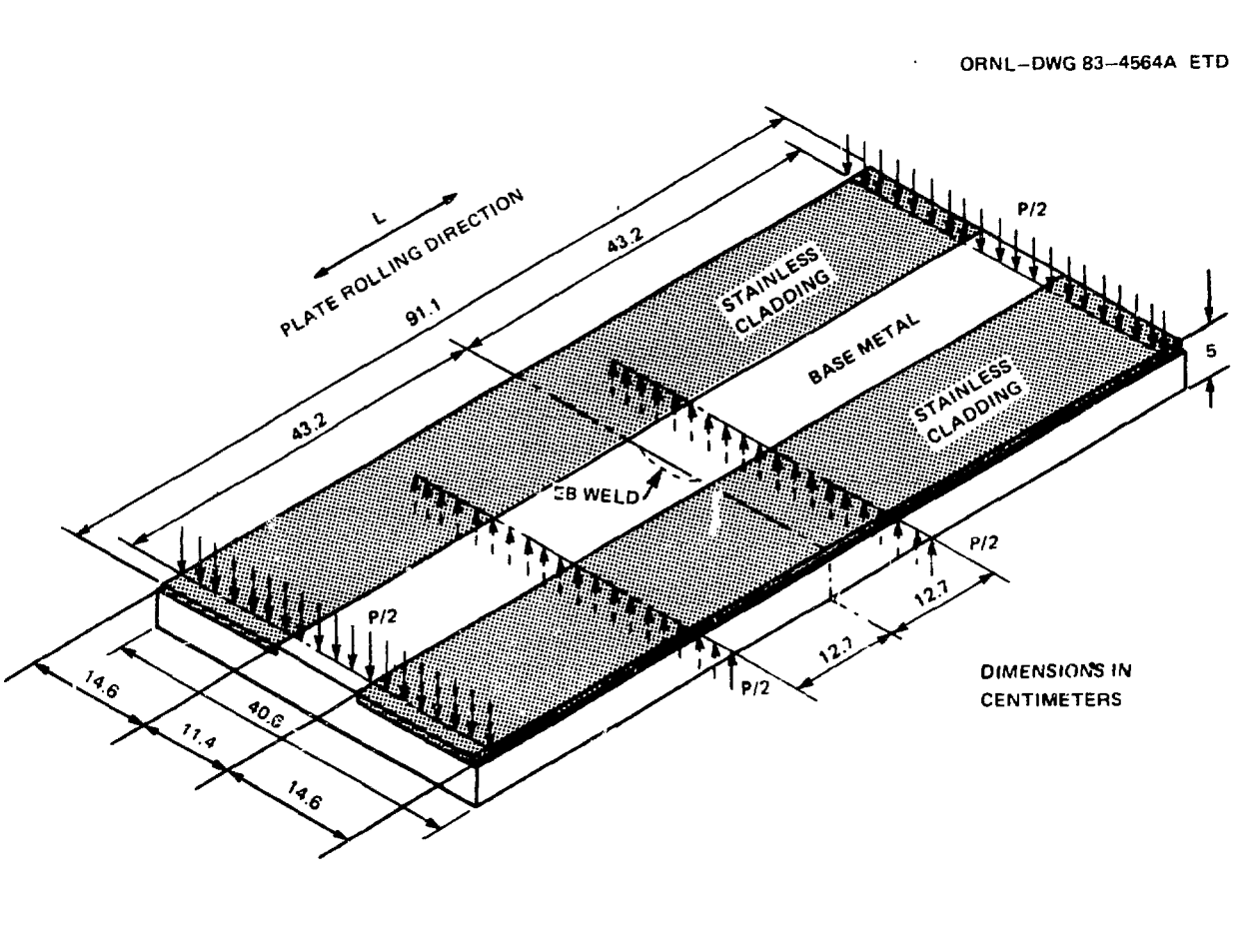
ORNL–DWG 83–4564A ETD
L
PLATE ROLLING DIRECTION
91.1
43.2
43.2
STAINLESS CLADDING
BASE METAL
STAINLESS CLADDING
EB WELD
P/2
P/2
P/2
P/2
5
12.7
12.7
14.6
40.6
11.4
14.6
DIMENSIONS IN CENTIMETERS

FIG. 4

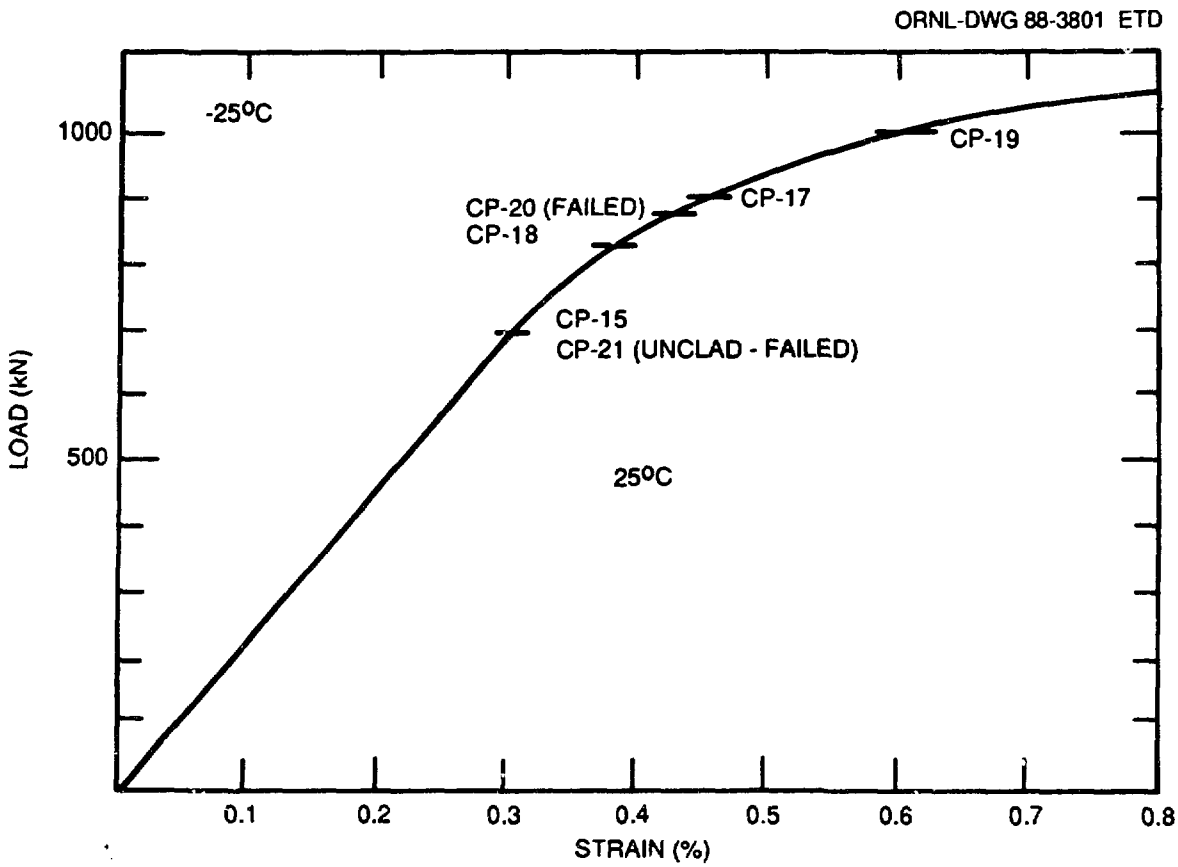
ORNL-DWG 88-3801 ETD
-25°C
1000
500
LOAD (kN)
CP-19
CP-17
CP-20 (FAILED)
CP-18
CP-15
CP-21 (UNCLAD - FAILED)
25°C
0.1
0.2
0.3
0.4
0.5
0.6
0.7
0.8
STRAIN (%)

CLAD PLATES HAVE MAINTAINED STRUCTURAL INTEGRITY AT LOADS THAT HAVE RUPTURED AN UNCLAD PLATE TEST TEMPERATURE: (NDT-10)°C

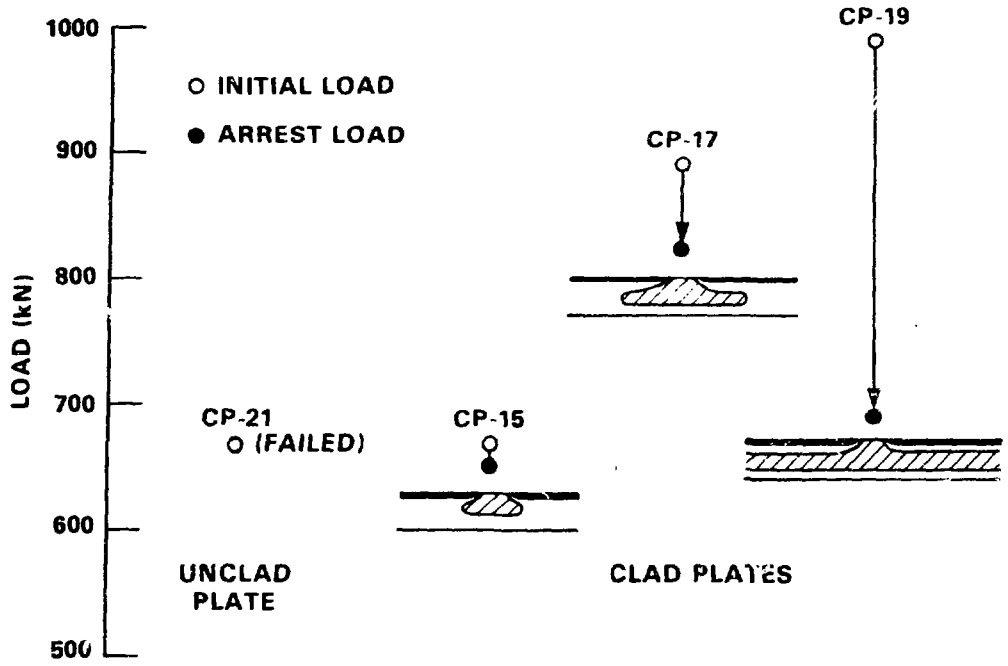

FIG. 5

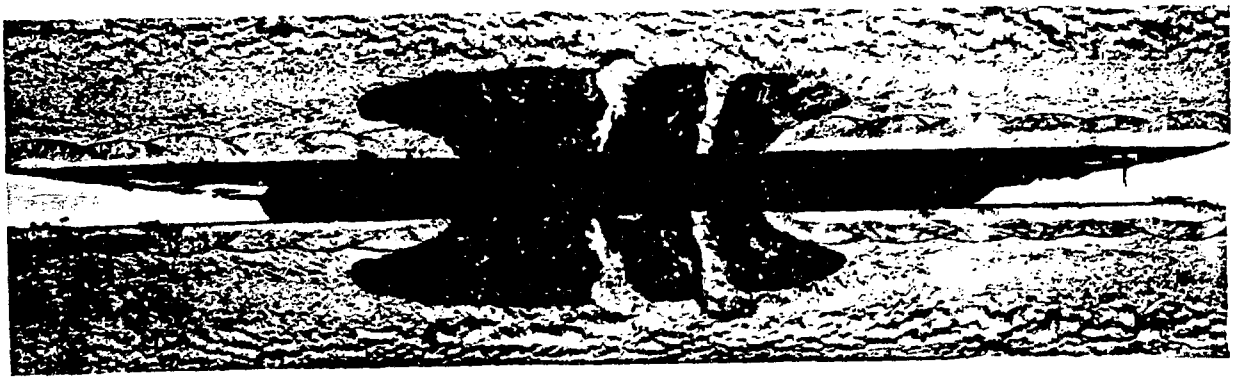

FIG. 6

FIG. 7.

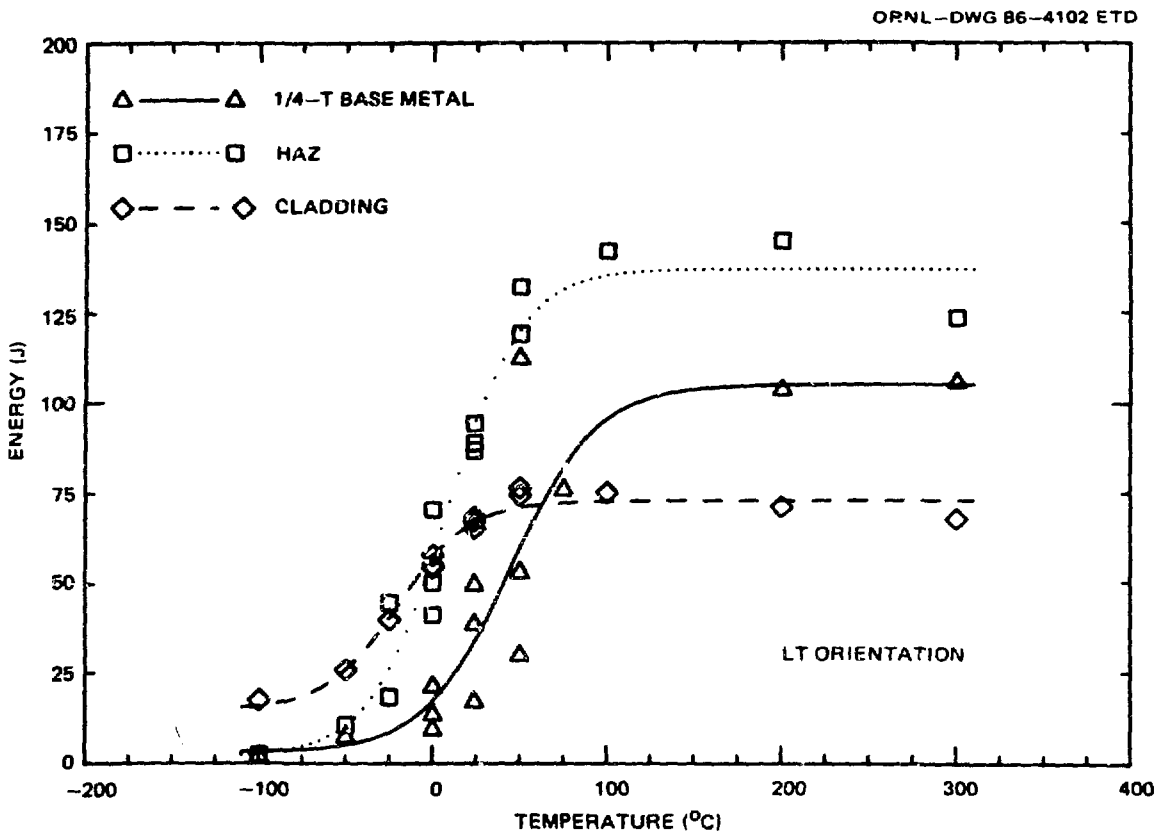
ORNL–DWG 86–4102 ETD
1/4–T BASE METAL
HAZ
CLADDING
LT ORIENTATION
ENERGY (J)
TEMPERATURE (°C)
200
175
150
125
100
75
50
25
0
–200
–100
0
100
200
300
400